JOURNAL OF Materials CHEMISTRY

Diversity in the $\frac{1}{2}$ spin arrangement of $[Ni(dmit)_2]^-$ anions in divalent Ca^{2+}(crown ether) supramolecular cation salts

Tomoyuki Akutagawa,*[a,b,c] Nobuhiro Takamatsu,[b] Kozo Shitagami,[b] Tatsuo Hasegawa,[a,b] Takayoshi Nakamura,*[a,b] Tamotsu Inabe,[d] Wataru Fujita[e] and Kunio Awaga[c,e]

[a]*Research Institute for Electronic Science, Hokkaido University, Sapporo 060-0812, Japan. E-mail: takuta@imd.es.hokudai.ac.jp; Fax: +81-11-706-4972; Tel: +81-11-706-2884*
[b]*Graduate School of Environmental Earth Science, Hokkaido University, Sapporo 060-0810, Japan*
[c]*PRESTO, Japan Science and Technology Corporation (JST), Japan*
[d]*Graduate School of Science, Hokkaido University, Sapporo 060-0810, Japan*
[e]*Graduate School of Arts and Science, The University of Tokyo, Meguro 153-8902, Japan*

Received 27th February 2001, Accepted 2nd May 2001
First published as an Advance Article on the web 30th May 2001

Calcium ion (Ca^{2+}) and crown ethers, 12-crown-4, 15-crown-5, 1-aza-18-crown-6 (A18-crown-6) and 1,10-diaza-18-crown-6 (DA18-crown-6), were assembled into divalent supramolecular cation (SC^{2+}) structures in the monovalent $[Ni(dmit)_2]^-$ salts ($dmit^{2-}$ = 2-thioxo-1,3-dithiole-4,5-dithiolate), which regulate the arrangement of the $[Ni(dmit)_2]^-$ anions in the crystal. The divalent SC^{2+}–$[Ni(dmit)_2]^-$ system showed a larger diversity of crystal structures compared with the monovalent SC^+ system. Peculiar magnetic behavior was observed depending on the arrangement of the $S=\frac{1}{2}$ spins on the $[Ni(dmit)_2]^-$ anions. Single crystals of Ca^{2+}(12-crown-4)$_2$[Ni(dmit)$_2$]$_2$ (**1**) and Ca^{2+}(15-crown-5)$_2$[Ni(dmit)$_2$]$_2$(CH_3CN)$_{0.7}$ (**2**) had a typical sandwich-type Ca^{2+}(crown ether)$_2$ structure, which included the formation of π–π dimers and monomers of $[Ni(dmit)_2]^-$ anions in the crystal. The temperature-dependent magnetic susceptibility (χ_m) of salt **1** showed a magnetic transition at 190 K, at which temperature the spins on each $[Ni(dmit)_2]^-$ dimer formed a singlet pair. On the other hand, the magnetic behavior of salt **2** obeyed the Curie–Weiss law. The Ca^{2+} ions in the isostructural single crystals of Ca^{2+}(A18-crown-6)[Ni(dmit)$_2$]$_2$(CH_3CN)$_2$ (**3**) and Ca^{2+}(DA18-crown-6)[Ni(dmit)$_2$]$_2$(CH_3CN)$_2$ (**4**) were completely included into the 18-crown-6 cavity, and further interacted with two CH_3CN molecules from the axial position. The resultant Ca^{2+}(18-crown-6)(CH_3CN)$_2$ cations induced the formation of uniform zig-zag chains of the $[Ni(dmit)_2]^-$ anions, the magnetic susceptibility of which were explained by a one-dimensional Heisenberg antiferromagnetic linear chain. The magnetism of these salts was discussed in terms of the intermolecular transfer integral *t*.

Transition metal complexes of $dmit^{2-}$ (2-thioxo-1,3-dithiole-4,5-dithiolate) ligands have been utilized to obtain molecular conductors, superconductors, magnets and nonlinear optical materials.[1] The discovery of a superconducting transition in (TTF)[Ni(dmit)$_2$]$_2$ remarkably progressed the studies on electrically conducting [Ni(dmit)$_2$] salts.[2] The partially oxidized electronic state of the $[Ni(dmit)_2]^{\delta-}$ molecule ($\delta<1$) is essential for the high conductivity, which is easily realized by chemical or electrochemical oxidation of the monovalent $[Ni(dmit)_2]^-$ anion.[1–3] On the other hand, the monovalent $[Ni(dmit)_2]^-$ anion has an open-shell electronic structure bearing an $S=\frac{1}{2}$ spin, and thus, is a useful building block for molecular magnets. The magnetic exchange interaction *J* is determined by the transfer integral *t* and on-site Coulomb repulsion *U*, $J\sim t^2/U$. Therefore, the side-by-side intermolecular S–S interaction in addition to the face-to-face π–π stack can be utilized to regulate the magnetic interactions between $[Ni(dmit)_2]^-$ anions in the crystal.[4] Although the ratio of *t* between the intermolecular π–π and side-by-side S–S interactions of [Ni(dmit)$_2$] molecules is typically observed in the range from 5 : 1 to 100 : 1, the side-by-side S–S interaction possibly increases the multi-dimensional magnetic interaction. Regulation of the $[Ni(dmit)_2]^-$ arrangements in the crystal is essential for designing [Ni(dmit)$_2$]-based molecular magnets.

Several types of magnetism of [Ni(dmit)$_2$]-based molecular crystals have been reported, namely, i) antiferromagnetic interactions in (M^{2+})(cyclam)[Ni(dmit)$_2$]$_2$(CH_3CN) ($M^{2+}=Cu^{2+}$ and Ni^{2+})[5] and [Ni(Me_5C_5)$_2$][Ni(dmit)$_2$] (Me_5C_5 = pentamethylcyclopentadienyl);[6] ii) ferromagnetic interactions in [Fe(Me_5C_5)$_2$][Ni(dmit)$_2$];[7] iii) spin-ladder chains in (EPYNN$^+$)[Ni(dmit)$_2$]$^-$ (EPYNN$^+$ = *p*-*N*-ethylpyridinium nitronyl nitroxide)[8] and iv) ferromagnetic ordering in [Mn(Me_5C_5)$_2$][Ni(dmit)$_2$] below 2.5 K.[6] The crystal structure as well as the mechanism of ferromagnetic ordering of the last compound are not yet clear.

Counter cations are necessary to neutralize the charge of the $[Ni(dmit)_2]^-$ in the crystal.[1–3] The salts listed above have magnetic moments arising from the counter cations of transition metal ions or organic neutral radicals, which behave as free spins for the (M^{2+})(cyclam) and show a ferromagnetic interaction in the case of EPYNN$^+$. The origin of the ferromagnetic interaction in the [Fe(Me_5C_5)$_2$][Ni(dmit)$_2$] has been interpreted as a charge-transfer excitation between the donor [Fe(Me_5C_5)$_2$] and acceptor $[Ni(dmit)_2]^-$. We have introduced supramolecular cation (SC) units as the counter cation of $[Ni(dmit)_2]^-$ salts.[9–11] By using the SC approach, we can regulate the [Ni(dmit)$_2$] assembly, and, thus, can control the electrical and magnetic properties of the [Ni(dmit)$_2$] salts. In the case of conducting salts, the monovalent SC^+ units, M^+(crown ethers), were effective in modulating the π–π stacking mode and side-by-side S–S interaction of the $[Ni(dmit)_2]^{\delta-}$ molecules.[9] The sandwich-type M^+(12-crown-4)$_2$ and planar, disc-shaped M^+(18-crown-6) SC^+ structures gave dimers and trimers of [Ni(dmit)$_2$] molecules, respectively,

 DOI: 10.1039/b101873f

within the electrically conducting column.[9g,11] Furthermore, the ionic channel structures were constructed from the regular array of crown ethers in the $(Li^+)_{0.6}$(15-crown-5)[Ni(dmit)$_2$]$_2$(H_2O) and $(M^+)_x$(18-crown-6)[Ni(dmit)$_2$]$_2$ ($M^+ = Li^+$, Na^+ and Cs^+) salts.[10,11]

In preliminary studies, we demonstrated the regulation of the [Ni(dmit)$_2$]$^-$ anions by using monovalent SC^+ structures. The planar, disc-shaped M^+(DA18-crown-6) cations ($M^+ = K^+$ and Rb^+ and DA18-crown-6 is 1,10-diaza-18-crown-6) in the M^+(DA18-crown-6)[Ni(dmit)$_2$]$^-$ salts induced the formation of uniform [Ni(dmit)$_2$]$^-$ chains, which show one-dimensional Heisenberg antiferromagnetic behavior.[12] The planar, disc-shaped M^+(DA18-crown-6) cations prevent the π–π interaction of [Ni(dmit)$_2$]$^-$ anions, which results in the [Ni(dmit)$_2$]$^-$ chain through the side-by-side S–S interactions. The barrel-type [NH_4^+(15-crown-5)$_2$]$_2$ cation caused the [Ni(dmit)$_2$]$^-$ anions to form a dimer chain, the magnetism of which was explained by Curie–Weiss behavior.[12] The SC^+ approach made it possible to design the cation structure and [Ni(dmit)$_2$] arrangement in the crystals.[13]

One of the largest factors determining the crystal structure of ionic crystals is the electrostatic Madelung energy. Monovalent M^+X^- inorganic crystals show typical crystal structures of NaCl- and CsCl-types, while the divalent $M^{2+}(X^-)_2$ crystals exhibit structural diversity, *e.g.*, fluorite (CaF_2), anti-fluorite (Na_2O), rutile ($CaCl_2$) and CdI_2 *etc.*, because of the larger coordination freedom in MX_2-type salts than in MX-type.[14] In this study, we used various crown ethers for binding Ca^{2+}, and present the structures and magnetic properties of the following crystals; Ca^{2+}(12-crown-4)$_2$[Ni(dmit)$_2$]$_2$ (**1**), Ca^{2+}(15-crown-5)$_2$[Ni(dmit)$_2$]$_2$(CH_3CN)$_{0.7}$ (**2**), Ca^{2+}(A18-crown-6)[Ni(dmit)$_2$]$_2$-(CH_3CN)$_2$ (**3**) and Ca^{2+}(DA18-crown-6)[Ni(dmit)$_2$]$_2$(CH_3CN)$_2$ (**4**) (Scheme 1).[15] A preliminary study on salts **4** has appeared in ref. 15.

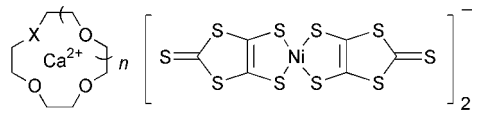

1: n = 1, X = O
2: n = 2, X = O
3: n = 3, X = NH

Scheme 1

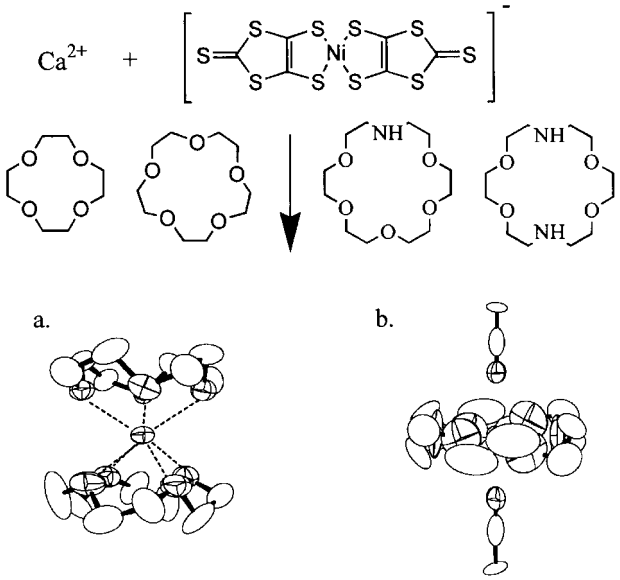

Fig. 1 Divalent supramolecular cation (SC^{2+}) structures of a) sandwich-type Ca^{2+}(12-crown-4)$_2$ and b) Ca^{2+}(A18-crown-6)-(CH_3CN)$_2$.

Results and discussion

Crystal structures

The salts **1**–**4** have quite complex crystal structures compared with the monovalent M^+(crown ethers)[Ni(dmit)$_2$] salts. Table 1 summarizes the crystal data of the salts **1**–**4**.

Supramolecular cation structures

Calcium ions (Ca^{2+}) and 12-crown-4 or 15-crown-5 are assembled into the sandwich-type SC^{2+} structures of Ca^{2+}(12-crown-4)$_2$ and Ca^{2+}(15-crown-5)$_2$ in salts **1** and **2** (Fig. 1a). That the ionic radius of Ca^{2+} (0.99 Å) is larger than the radius of the cavity in 12-crown-4 (0.6–0.75 Å) causes a sandwich-type coordination to Ca^{2+} ion.[16] Although the ionic radius of Ca^{2+} fits well in the cavity of 15-crown-5 (0.85–1.25 Å), the sandwich-type SC^{2+} structure is obtained in the salt **2** rather than a disc-shaped structure. Similar sandwich-type structures have been observed in Ca^{2+}(12-crown-4)$_2$(SCN^-)$_2$ and Ca^{2+}(15-crown-5)$_2$(SCN^-)$_2$ salts.[17] The

Table 1 Crystal data, data collection, and reduction parameter of the salts **1**–**4**

	1	**1**	**2**	**3**	**4**[a]
Chemical formula	$C_{28}H_{32}O_8S_{20}CaNi_2$	$C_{28}H_{32}O_8S_{20}CaNi_2$	$C_{100}H_{126}N_2O_{30}S_{60}Ca_3Ni_6$	$C_{28}H_{31}S_{20}N_3O_5CaNi_2$	$C_{28}H_{32}N_4O_4S_{20}CaNi_2$
Formula weight	1295.24	1295.24	4232.13	1288.25	1287.27
Space group	$P2_1/n$ (no. 14)	$P2_1/n$ (no. 14)	$P\bar{1}$ (no. 2)	$P4_2/mnm$ (no. 136)	$P4_2/mnm$ (no. 136)
a/Å	19.872(1)	19.8366(4)	12.4442(2)	15.598(3)	15.562(1)
b/Å	19.7547(8)	19.5053(3)	12.5299(2)		
c/Å	12.6242(6)	12.5358(2)	26.872(1)	10.222(4)	10.218(2)
α/deg			97.0670(7)		
β/deg	95.442(1)	94.7610(7)	91.7234(8)		
γ/deg			97.214(1)		
V/Å^3	4933.55(4)	4833.6(1)	4120.8(2)	2486.9(6)	2474.7(3)
Z	4	4	1	2	2
ρ_{calc}/g cm^{-3}	1.744	1.780	1.61	1.72	1.73
T	297	150	297	297	297
μ/cm^{-1}	17.56	17.93	15.76	17.39	17.47
No. of reflections measured	10878	11401	56890	1706	1581
No. of independent reflections	10883	11063	18781	1593	1204
No. of reflections used	4662	8538	10905	947	1046
R^b	0.041	0.023	0.049	0.050	0.046
$R_w(F^2)^b$	0.050	0.037	0.126	0.081	0.035

[a]From ref. 15. [b]$R = \Sigma||F_o|-|F_c||/\Sigma|F_o|$ and $R_w = (\Sigma\omega(|F_o|-|F_c|)^2/\Sigma\omega F_o^2)^{\frac{1}{2}}$.

average Ca^{2+}–O distance (2.43 Å) in salt **1** is 0.08 Å shorter than the sum of ion and van der Waals (vdW) contact (2.51 Å), while that (2.66 Å) in salt **2** is 0.15 Å longer than the sum of ion and vdW contact.[18]

Because the ionic radius of Ca^{2+} is smaller than the radius of the cavity in 18-crown-6 (1.3–1.6 Å), the Ca^{2+} ions are completely included in the A18-crown-6 and DA18-crown-6 cavities in salts **3** and **4**. Further interaction of the Ca^{2+} at the axial position with two CH_3CN molecules results in the Ca^{2+}(A18-crown-6)$(CH_3CN)_2$ and Ca^{2+}(DA18-crown-6)-$(CH_3CN)_2$ structures (Fig. 1b). The Ca^{2+} ions are loosely connected in the large 18-crown-6 cavity, and the average Ca^{2+}–O distances in salts **3** (2.57 Å) and **4** (2.58 Å) are about 0.1 Å longer than the sum of the ion and vdW contacts.[18]

Ca^{2+}(12-crown-4)$_2$[Ni(dmit)$_2$]$_2$ (1)

One Ca^{2+}(12-crown-4)$_2$ cation and two [Ni(dmit)$_2$] (**A** and **B**) anions are the crystallographically asymmetric unit in salt **1**. Figs. 2a and 2b show the unit cell viewed along the *c*- and *a*-axis, respectively. The crystal is constructed from the π–π dimers of $[Ni(dmit)_2]^-$ **A**–**A** and isolated monomers of **B**. The **A**–**A** dimers are connected by side-by-side S–S contacts along the *a*-axis (Fig. 2a). The intermolecular π–π interaction in **A**–**A** dimer ($t_1 = 8.96$) is quite significantly larger than the interdimer S–S interaction ($t_2 = 0.60$) at 297 K. The long axis of the **B** molecule is orthogonal to the molecular plane of the **A**–**A** dimer, and four **B** molecules form a rhombus arrangement in the *bc*-plane (Fig. 2b). The π–π overlap in **B**–**B** ($t_3 = -3.47$) is the second largest intermolecular interaction in the crystal. The **A**–**A** dimer has weak intermolecular interactions with the orthogonal **B** molecule ($t_4 \sim 1.2$). The **A**–**A** dimer and monomer **B** interact with each other through the orthogonal S–S interactions (Fig. 2). This orthogonal S–S interaction mode is typically observed in the divalent SC^{2+}–[Ni(dmit)$_2$]$_2$ systems. The sandwich-type SC^{2+} units exist at the space above the π-plane of the **B** molecule and are surrounded by four **A**–**A** dimer units without effective intermolecular interactions (dotted circle in Fig. 2b).

Ca^{2+}(15-crown-5)$_2$[Ni(dmit)$_2$]$_2$(CH_3CN)$_{0.7}$ (2)

One and a half Ca^{2+}(15-crown-5)$_2$ units, three [Ni(dmit)$_2$] (**A**, **B** and **C**) and one CH_3CN molecule are the crystallographically asymmetric units in the salt **2**. Figs. 3a and 3b show the unit cell viewed along the *a*- and *c*-axis, respectively. The **A** and **B** molecules form two independent π–π dimers of **A**–**A** and **B**–**B**, respectively. Since π–π dimerization in the **A**–**A** unit is only observed at the terminal sulfur atom of $[Ni(dmit)_2]^-$, the magnitude of the π–π dimerization in the **A**–**A** unit ($t_1 = 2.54$) is half of that in **B**–**B** ($t_1' = 5.67$). The quite smaller magnitude of the π–π dimerizations in salt **2** than that in salt **1** reflects the weak magnetic interaction within the dimer unit.

The interdimer side-by-side S–S contacts observed along the *c*-axis ($t_2 = -0.18$ and $t_2' = -0.11$) are quite significantly smaller than those of the intradimer. Another interdimer side-by-side S–S interaction between the **A**–**A** and **B**–**B** dimers ($t_3 = 0.41$) along the $a+b$-axis is also insufficient to increase the magnetic interaction. The long axis of the **C** molecule is orthogonal to the long axis of the **A**–**A** and **B**–**B** dimers as seen in salt **1**, which is arranged along the $a+b$-axis. The orthogonal S–S interactions of the **A**–**C** and **B**–**C** molecules (Fig. 3c) connect each dimer weakly ($t_4 \sim 0.5$). The sandwich-type SC^{2+} units exist at the space above the π-plane of **C** molecule and are arranged along the $a+b$-axis without intermolecular interactions (dotted circles in Fig. 3b).

Ca^{2+}(A18-crown-6)[Ni(dmit)$_2$]$_2$(CH_3CN)$_2$ (3)

The crystals of salts **3** and **4** are isostructural with each other, thus we will describe the crystal structure of salt **3**. A quarter unit of $[Ni(dmit)_2]^-$ is the crystallographically asymmetric unit. Figs. 4a and 4b show the unit cell of salt **3** viewed along the *c*- and $a+b$-axis, respectively. The molecular plane of the $[Ni(dmit)_2]^-$ anions is orthogonal to the *ab*-plane, and the $[Ni(dmit)_2]^-$ anions form a parallel-cross lattice. The long axes of $[Ni(dmit)_2]^-$ anions within the same plane are parallel to each other and are orthogonal to that of the next layer.

The $[Ni(dmit)_2]^-$ anions form a uniform zig-zag chain along the $a+b$ and $a-b$ axis through the π–π overlap ($t_1 = 4.26$) between the terminal sulfur atoms. The interchain contacts are not observed within the same *ab*-plane. These π–π chains are weakly connected through the orthogonal S–S interactions ($t_2 = 0.61$) along the *c*-axis (Fig. 4b). The magnitude of the intermolecular interactions ($t_1 = 3.71$ and $t_2 = 0.89$) in salt **4** is the same range as that of salt **3**. From the magnitude of the t_1 and t_2 interactions, the intermolecular interaction in salts **3** and **4** is dominant in the uniform, one-dimensional zig-zag chain direction of the $[Ni(dmit)_2]^-$ anions.

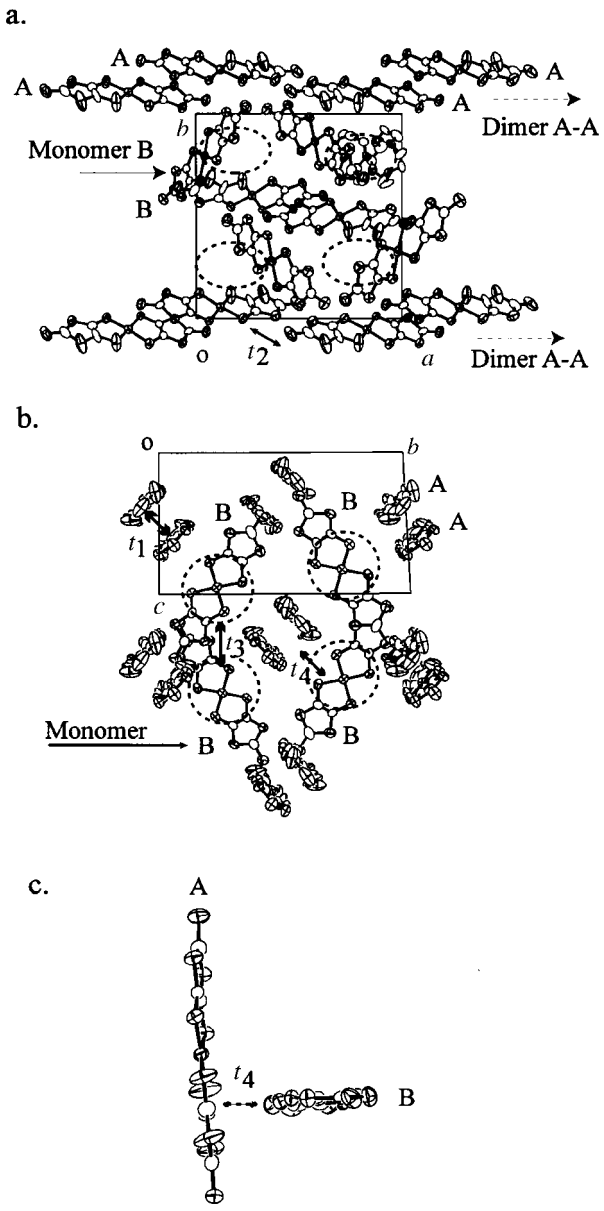

Fig. 2 Crystal structure of Ca^{+}(12-crown-4)$_2$[Ni(dmit)$_2$]$_2$ (**1**) viewed along a) the *c*-axis and b) the *a*-axis. The **A**–**A** dimers are arranged along the *a*-axis. The transfer intergrals of interdimer (t_1) and intradimer (t_2 and t_3) are shown. A part of Ca^{2+}(12-crown-4)$_2$ units is omitted and schematically drawn.

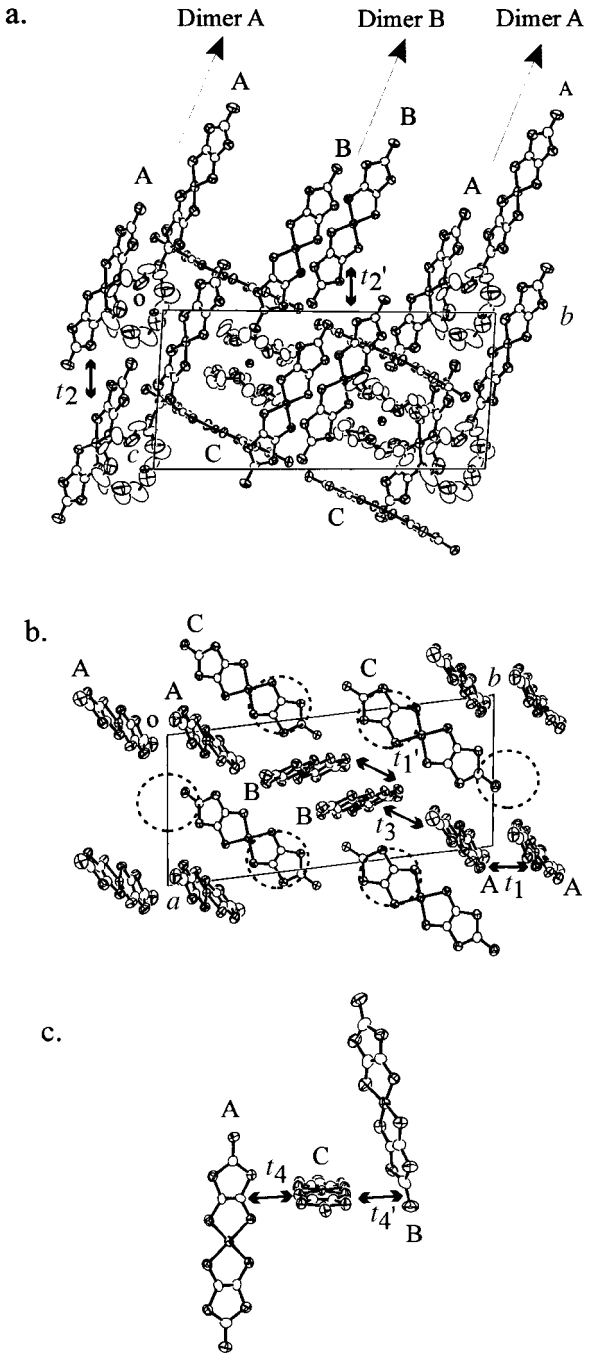

Fig. 3 Crystal structure of $Ca^{+}(15\text{-crown-}5)_2[Ni(dmit)_2]_2(CH_3CN)_{0.7}$ (**2**) viewed along a) the *a*-axis and b) the *c*-axis. Dimer chains of **A**–**A** and **B**–**B** are elongated along the *c*-axis, and the monomer **C** is arranged normal to the molecular plane of the dimers. The intradimer transfer integrals in **A**–**A** and **B**–**B** units are t_1 and t_1', respectively. The SC^{2+} structures are drawn in schematically.

$[Ni(dmit)_2]^-$ Anion arrangement and magnetism

Fig. 5 shows the temperature-dependent magnetic susceptibility (χ_m) of the salts **1**, **2** and **3**. The magnetic susceptibility of salt **4** was almost the same as that of salt **3**. We will discuss the magnetic properties of salts **1**–**4** in terms of the magnitude of t between the $[Ni(dmit)_2]^-$ anions. Table 2 summarizes the transfer integrals t of the $[Ni(dmit)_2]^-$ arrangements of salts **1**–**4**.

There are two different origins of magnetism: those arising from the dimers and the monomers of $[Ni(dmit)_2]$ in salt **1**. The χ_m value of salt **1** increases monotonically by lowering the temperature from 350 to 190 K, then a sudden decrease in the χ_m value is observed at 190 K. The transition is reversible

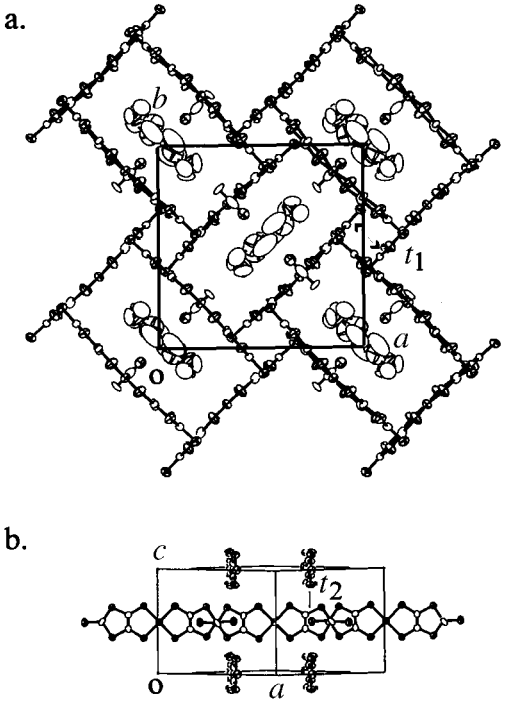

Fig. 4 a) Crystal structure of $Ca^{2+}(A\text{-}18\text{-crown-}6)[Ni(dmit)_2]_2(CH_3CN)_2$ (**3**) viewed along the *c*-axis. b) Linear zig-zag $[Ni(dmit)_2]^-$ chain viewed along the $a+b$-axis. The transfer integrals in the linear π–π overlap and side-by-side S–S contact are t_1 and t_2, respectively.

and is accompanied by a small hysteresis (~3 K) against the temperature cycle. The magnetic moment above 190 K is almost constant ($\chi_m T = 0.7$ emu K mol^{-1}), which is consistent with two free $S=\frac{1}{2}$ spins ($g \sim 2$) per unit cell. On the other hand, the $\chi_m T$ value below 190 K ($\chi_m T = 0.2 \sim 0.4$ emu K mol^{-1}) are gradually decreased by a lowering of temperature, which corresponds to the antiferromagnetic interaction between the monomers.

Fig. 6 shows the temperature-dependent lattice parameters of salt **1** in the temperature range from 100 to 310 K. The lattice constants of $a = 19.891$, $b = 19.737$ and $c = 12.603$ Å at 310 K decreased with the decrease in temperature down to 190 K. A discontinuous change in the lattice parameter is clearly observed at 190 K along the *a*-axis, which corresponds to the **A**–**A** dimer chain direction.

The crystal of salt **1** at 150 K has the same crystal symmetry as at 297 K. However, the magnitude of the π–π dimer interaction in the **A**–**A** unit is significantly different. The intradimer t_1 interaction at 150 K (11.34) is *ca.* 30% larger than that at 297 K, although the interdimer interaction ($t_2 = 0.74$) at 150 K is of similar magnitude to that at 297 K. In contrast, the **B**–**B** interaction in the rhombic lattice is slightly reduced from $t_3 = -3.47$ (297 K) to $t_3 = -2.21$ (150 K). The increase in π–π dimerization in the **A**–**A** unit is the origin of the discontinuous lattice change in the *a*-axis and of the magnetic transition at 190 K.

The magnetic exchange energy J within the dimer at 150 K is 1.5 times larger than that at 297 K from a proportional relation of $J \propto t^2$, thus we can reasonably conclude that the magnetic transition at 190 K is due to the spin singlet formation of the **A**–**A** dimer. The spin from monomer **B** contributes to the magnetism below 190 K, however, quantitative analysis of this magnetic interaction has not been achieved.

The temperature-dependent χ_m behavior observed in salt **2** obeys the Curie–Weiss law in the temperature range from 40 to 350 K (Fig. 5b). The almost constant $\chi_m T$ value (0.73 emu K mol^{-1}) suggests the absence of effective magnetic interaction between the $[Ni(dmit)_2]^-$ anions above 40 K. Below

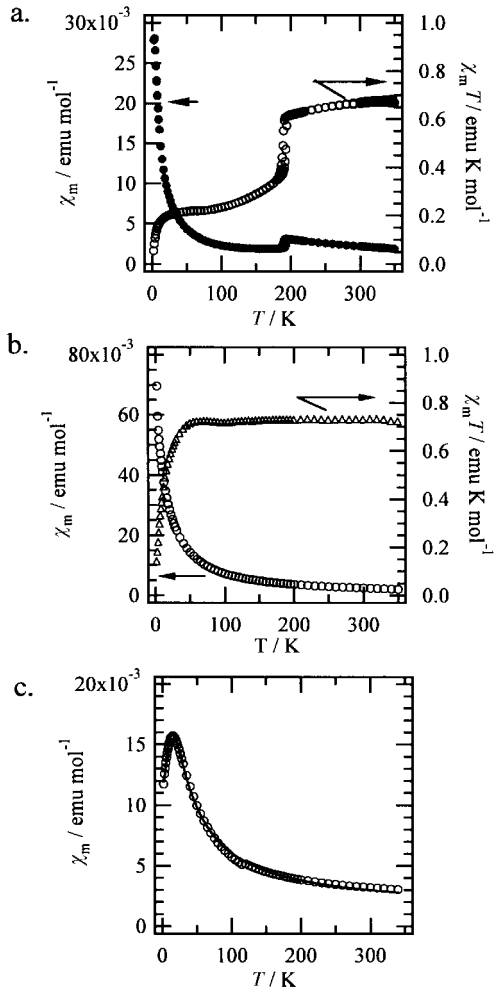

Fig. 5 Temperature-dependent magnetic susceptibility (χ_m/emu mol^{-1}) of a) **1**, b) **2** and c) **3**. The χ_m *vs.* T (left-scale) and $\chi_m T$ *vs.* T (right-scale) plots are drawn in same figure for salts **1** and **2**. The solid line in Fig. 5c is the fitting curve using the one-dimensional Heisenberg antiferromagnetic linear chain model (2 K $< T <$ 350 K).

40 K, a weak antiferromagnetic interaction is observed as a gradual drop in the $\chi_m T$ value ($\theta = -8.5$ K). Since the magnitude of the intradimer π–π interaction in salt **2** is quite significantly smaller than that observed in salt **1**, the formation of a singlet pair on the **A**–**A** or **B**–**B** dimers is not observed.

The temperature-dependent χ_m of salt **3** has a broad χ_m maximum at around 15 K, and the behavior is well fitted by the one-dimensional Heisenberg antiferromagnetic linear chain model (solid line in Fig. 5c).[19] The uniform zig-zag chain of $[Ni(dmit)_2]^-$ anions, as confirmed by X-ray crystal structural analysis, is consistent with the temperature-dependent magnetic behavior. The intrachain magnetic exchange energy ($J/k_B = -11.7$ K) estimated from the fitting result in salt **3** is almost the same magnitude as that in salt **4** ($J/k_B = -12.2$ K). The regular π–π interaction ($t \sim 4$) of the $[Ni(dmit)_2]^-$ anions in salts **3** and **4** is the origin of the antiferromagnetic interaction with the magnetic exchange energy of $|J/k_B| \sim 10$ K.

Table 2 Packing mode and transfer integral ($t \times 10^{-2}$ eV)[a] in salts **1**–**4**

	1	**1′**[b]	**2**[c]	**3**	**4**
Packing mode [d]	D–M	D–M	D–M	Regular	Regular
t_1	8.96	11.34	2.54, 5.67	4.26	3.71
t_2	0.06	0.74	−0.18, −0.11	0.61	0.89
t_3	−3.47	−2.21	−0.41	—	—
t_4	1.2	1.4	−0.5	—	—

[a]The transfer integrals (t) were obtained by the LUMO of $[Ni(dmit)_2]^-$ based on extended Hückel calculations ($t = -10S$ eV, S is the overlap integral). [b]Based on the crystal structure at 150 K. [c]Two kinds of transfer integrals for **A**–**A** and **B**–**B** dimers are shown in the left and right of the column, respectively. [d]Dimers (D) and monomers (M) coexist in the crystal.

Fig. 7 summarizes the intermolecular interaction modes of the $[Ni(dmit)_2]^-$ anions observed in the monovalent M^+(crown ethers)$[Ni(dmit)_2]^-$ (upper two in refs. 9*b* and 12) and in the divalent Ca^{2+}(crown ethers)$[Ni(dmit)_2]_2$ (lower six in the present study) together with the orthogonal S–S interactions. NH_4^+(15-crown-5)$_2$[Ni(dmit)$_2$] forms a π–π dimer with an interdimer interaction of $t \sim 5$, while M^+(DA18-crown-6)[Ni(dmit)$_2$] ($M^+ = K^+$ and Rb^+) has a regular [Ni(dmit)$_2$] chain with an intermolecular interaction of $t \sim 2$ through the terminal S–S interactions. The orthogonal arrangement of the $[Ni(dmit)_2]^-$ anions was not observed in the monovalent SC^+ system. The temperature-dependent magnetic behavior of these monovalent SC^+ salts was well fitted by the Curie–Weiss equation and one-dimensional Heisenberg antiferromagnetic linear chain model, respectively. The magnitude of π–π dimerization in NH_4^+(15-crown-5)$_2$[Ni(dmit)$_2$] is not strong enough to stabilize the singlet pair.

The divalent Ca^{2+}(crown ethers)$[Ni(dmit)_2]_2$ salts have much structural diversity and greater π–π interactions than those of the monovalent system. The magnitude of the transfer integrals in π–π interactions ranges from $t \sim 3$ to $t \sim 11$ for the Ca^{2+}(crown ethers)$[Ni(dmit)_2]_2$ system, which results in a variety of types of magnetism in these divalent salts. In particular, singlet pair formation of the spins between the dimer was observed when $t > 10$. Further, a novel π–π overlap mode with 120° bending of the long axis of the $[Ni(dmit)_2]^-$ anions is observed in the **B**–**B** overlap in salt **1** ($t \sim 3$), the π–π interaction mode of which resembles the two-dimensional molecular conductor of α-$(C_2H_5)_2(CH_3)_2N[Ni(dmit)_2]_2$ ($t \sim 7$).[20] The orthogonal S–S interactions are characteristic of the divalent SC^{2+} system, in which the long axes of the $[Ni(dmit)_2]^-$ anions are orthogonal to each other. The magnitude of the orthogonal S–S interactions found in salts **1**–**4** covers the t range from 0.5 to 2, the absolute value of which is not as large as those of the intradimer interactions. However, such anisotropic S–S interactions should be important for connecting the magnetic interactions over the crystal. The planar $[Ni(dmit)_2]^-$ anion has three types of intermolecular interaction modes: π–π overlap, side-by-side S–S and orthogonal S–S contacts through the peripherally substituted sulfur atoms. Crystal design using divalent SC^{2+} systems is effective in increasing the structural and magnetic diversity of the [Ni(dmit)$_2$]-based molecular magnets.

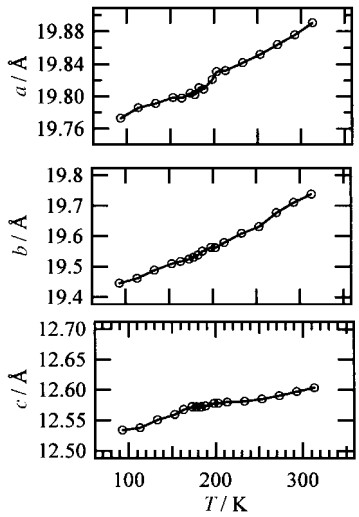

Fig. 6 Temperature-dependent lattice parameters (a, b and c) of salt **1** in the temperature range from 90 to 320 K.

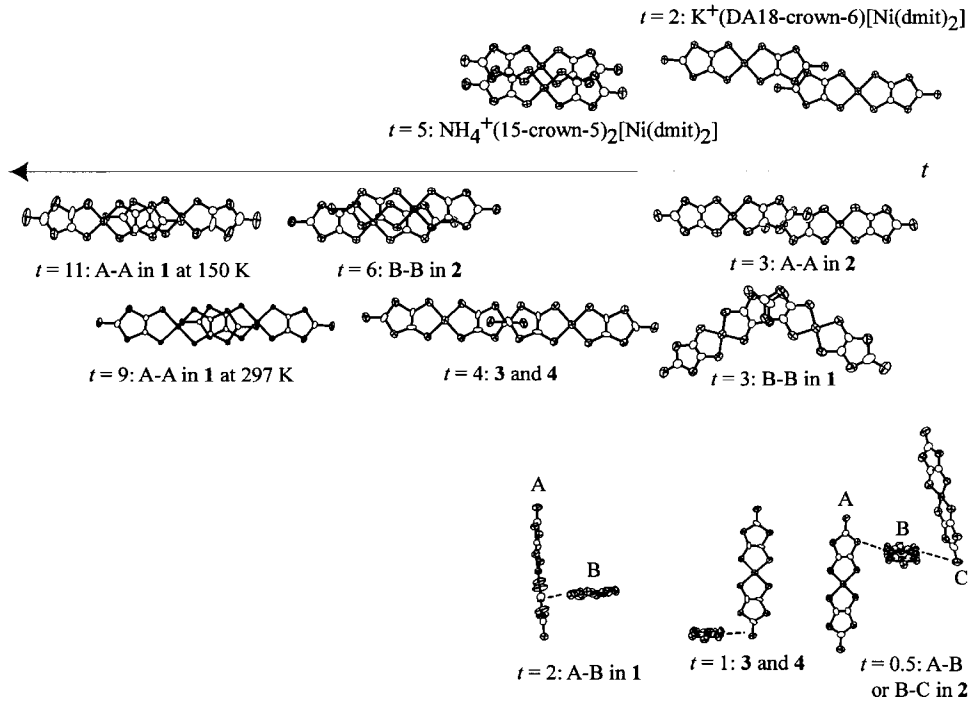

Fig. 7 Intermolecular interaction modes between the $[Ni(dmit)_2]^-$ anions and transfer integrals (t) observed in salts **1**–**4** and monovalent $SC^+[Ni(dmit)_2]$ salts of $NH_4^+(15\text{-crown-}5)_2[Ni(dmit)_2]$ and $K^+(DA18\text{-crown-}6)[Ni(dmit)_2]$.

Conclusion

Divalent $Ca^{2+}(\text{crown ethers})_x$ ($x=1$ or 2) supramolecular cation structures were assembled with the $[Ni(dmit)_2]^-$ anions bearing $S=\frac{1}{2}$ spin. By using divalent SC^{2+} structures, a diversity of structure as well as magnetic behavior of the $[Ni(dmit)_2]$ salts was observed, and the magnitude of the π–π interaction of the $[Ni(dmit)_2]$ anions covered a wide t range compared with those of the monovalent SC^+ salts (Fig. 7). Further design for obtaining novel magnetic properties of $[Ni(dmit)_2]$-based magnetic systems will be possible using the higher valence supramolecular cation system. For example, i) the trivalent supramolecular cations should further increase the structural diversity of the $[Ni(dmit)_2]^-$ anion arrangements and ii) trivalent magnetic lanthanide cations should provide the f–π magnetic spin systems.

Experimental

Crystal preparations

Monovalent (n-Bu_4N)$[Ni(dmit)_2]$ was prepared according to the literature.[21] The single crystals were grown using a slow diffusion method between the (n-Bu_4N)$[Ni(dmit)_2]$ and $Ca^{2+}(ClO_4^-)_2$–crown ethers in CH_3CN. The 12-crown-4, 15-crown-5, 18-crown-6, 1-aza-18-crown-6 (A18-crown-6) and 1,10-diaza-18-crown-6 (DA18crown6) were used as crown ethers. Cation exchange from n-Bu_4N to Ca^{2+}(crown ethers) occurred during crystal growth. Elemental analysis for salt **1**: found: C, 25.96; H, 2.38; N, 0%; $C_{28}H_{32}O_8S_{20}CaNi_2$ requires C, 25.96; H, 2.49; N, 0%; salt **2**: found: C, 28.69; H, 2.57; N, 0.37%; $C_{100}H_{126}N_2O_{30}S_{60}Ca_3Ni_6$ requires C, 28.39; H, 2.98; N, 0.66%; salt **3**: found: C, 26.33; H, 2.28; N, 3.52%; $C_{28}H_{31}S_{20}N_3O_5CaNi_2$ requires C, 26.10; H, 2.43; N, 3.26%.

Crystal structure determinations

Crystal data were collected on a Rigaku AFC-7R or a Raxis-Rapid diffractometer with Mo-Kα ($\lambda=0.71073$ Å) radiation using a graphite monochromator. The structures were solved and refined using the teXsan program.[22] The structure refinements were performed by the full matrix least-squares method. Table 1 summarizes the crystal data of salts **1**–**4**. Parameters were refined using the anisotropic temperature factors in all crystals, and the hydrogen atoms of salt **3** were removed from the refinements. A disordered arrangement of the nitrogen and oxygen atoms for the asymmetrical A18-crown-6 molecule was assumed in salt **3**.

Structural data have been deposited with the Cambridge Crystallographic Data Centre. CCDC reference numbers 15716–15719. See http://www.rsc.org/suppdata/jm/b1/b101873f/ for crystallographic files in .cif format.

Magnetic susceptibility

The temperature-dependent magnetic susceptibility was measured with a SQUID magnetometer (Quantum Design Model MPMS-5) for polycrystalline samples (30–40 mg). The magnetic field applied was 1 T for all measurements.

Calculations

The transfer integrals (t) were obtained within the tight-binding approximation using extended Hückel molecular orbital calculations. The LUMO of the $[Ni(dmit)_2]$ molecule was used as the basis function.[23] The semiempirical parameters for Slater-type atomic orbitals were taken from ref. 23. The t value between each pair of molecules is assumed to be proportional to the overlap integral (S) as $t=-10S$ eV.[23]

Acknowledgements

This work was partly supported by a Grant-in-Aid for Science Research from the Ministry of Education, Culture, Sports, Science and Technology of Japan and by the Proposal-Based New Industry Creative Type Technology R&D Promotion Program from the New Energy and Industrial Technology Development Organization (NEDO) in Japan. The authors thank Dr M. Wakeshima and Professor Y. Hinatsu for use of the SQUID magnetometer.

References

1 A. E. Pullen and R.-K. Olk, *Coord. Chem. Rev.*, 1999, **188**, 211.
2 (*a*) L. Brossard, M. Ribault, L. Valade and P. Cassoux, *Physica B+C (Amsterdam)*, 1986, **143**, 378; (*b*) L. Brossard, M. Ribault, L. Valade and P. Cassoux, *J. Phys. (Paris)*, 1989, **50**, 1521; (*c*) E. Canadell, *Coord. Chem. Rev.*, 1999, **185/186**, 629.
3 (*a*) *Handbook of Organic Conductive Molecules and Polymers Vol. 1*, ed. H. S. Nalwa, John Wiley & Sons, Chichester, 1997; (*b*) P. Cassoux, L. Valade, H. Kobayashi, A. Kobayashi, R. A. Clark and A. E. Underhill, *Coord. Chem. Rev.*, 1991, **110**, 115; (*c*) P. Cassoux, *Coord. Chem. Rev.*, 1999, **185/186**, 213.
4 (*a*) W. B. Heuer, A. E. True, P. N. Swepston and B. M. Hoffman, *Inorg. Chem.*, 1988, **27**, 1474; (*b*) W. B. Heuer, P. J. Squattrito, B. M. Hoffman and J. A. Ibers, *J. Am. Chem. Soc.*, 1988, **110**, 792.
5 H. Oshio, *Inorg. Chem.*, 1993, **32**, 4123.
6 C. Faulmann, A. E. Pullen, E. Riviere, Y. Journaux, L. Retailleau and P. Cassoux, *Synth. Met.*, 1999, **103**, 2296.
7 W. E. Broderick, J. A. Thompson, M. R. Godfrey, M. Sabat and B. M. Hoffman, *J. Am. Chem. Soc.*, 1989, **111**, 7657.
8 (*a*) H. Imai, T. Inabe, T. Otsuka, T. Okuno and K. Awaga, *Phys. Rev. B.*, 1996, **54**, 6838; (*b*) H. Imai, T. Otsuka, T. Naito, K. Awaga and T. Inabe, *J. Am. Chem. Soc.*, 1999, **121**, 8098.
9 (*a*) T. Akutagawa, T. Nakamura, T. Inabe and A. E. Underhill, *J. Mater. Chem.*, 1996, **7**, 135; (*b*) T. Akutagawa, T. Nakamura, T. Inabe and A. E. Underhill, *Thin Solid Films*, 1998, **331**, 264; (*c*) T. Akutagawa and T. Nakamura, *Coord. Chem. Rev.*, 2000, **198**, 297; (*d*) T. Akutagawa, Y. Nezu, T. Hasegawa, T. Nakamura, K. Sugiura, Y. Sakata, T. Inabe and A. E. Underhill, *Chem. Commun.*, 1998, 2599; (*e*) N. Robertson, T. Akutagawa, T. Nakamura, S. Roehrs and A. E. Underhill, *J. Mater. Chem.*, 1999, **9**, 1233; (*f*) T. Akutagawa, T. Hasegawa, T. Nakamura, T. Inabe, K. Sugiura, Y. Sakata and A. E. Underhill, *Synth. Met.*, 1999, **102**, 1747; (*g*) T. Akutagawa, T. Hasegawa, T. Nakamura, S. Takeda, T. Inabe, K. Sugiura, Y. Sakata and A. E. Underhill, *Inorg. Chem.*, 2000, **39**, 2645.
10 T. Nakamura, T. Akutagawa, K. Honda, A. E. Underhill, A. T. Coomber and R. H. Friend, *Nature*, 1998, **394**, 159.
11 T. Akutagawa, T. Hasegawa, T. Nakamura, S. Takeda, T. Inabe, K. Sugiura, Y. Sakata and A. E. Underhill, *Chem. Eur.J.*, 2001, in press.
12 (*a*) N. Takamatsu, T. Akutagawa, T. Hasegawa, T. Nakamura, T. Inabe, W. Fujita and K. Awaga, *Mol. Cryst. Liq. Cryst.*, 2000, **343**, 163; (*b*) N. Takamatsu, T. Akutagawa, T. Hasegawa, T. Nakamura, T. Inabe, W. Fujita and K. Awaga, *Inorg. Chem.*, 2000, **39**, 870.
13 T. Akutagawa, T. Hasegawa and T. Nakamura, *Handbook of Advanced Electronic and Photonic Materials and Devices*, ed. H. S. Nalwa, Academic Press, San Diego, 2000, **3**, 267.
14 A. R. West, *Basic Solid State Chemistry*, John Wiley & Sons, 1988.
15 T. Akutagawa, T. Nishihara, N. Takamatsu, T. Hasegawa, T. Nakamura and T. Inabe, *J. Phys. Chem. B*, 2000, **104**, 5871.
16 E. Weber, J. L. Toner, I. Goldberg, F. Vogtle, D. A. Laidler, J. F. Stoddart, R. A. Bartsch and C. L. Liotta, *Crown ethers and analogs*, eds. S. Patai and Z. Rappoport, John Wiley & Sons, New York, 1989.
17 (*a*) Y. Y. Wei, B. Tinant, J. -P. Declercq and M. V. Meerssche, *Acta Crystallogr., Sect. C: Cryst. Struct. Commun.*, 1988, **44**, 68; (*b*) Y. Y. Wei, B. Tinant, J. -P. Declercq and M. V. Meerssche, *Acta Crystallogr., Sect. C: Cryst. Struct. Commun.*, 1988, **44**, 73.
18 (*a*) A. Bondi, *J. Phys. Chem.*, 1964, **68**, 441; (*b*) A. F. Wells, *Structural Inorganic Chemistry*, 5th edn., Clarendon press, Oxford, 1984.
19 J. C. Bonner and M. E. Fisher, *Phys. Rev. A.*, 1964, **3**, 640.
20 R. Kato, H. Kobayashi, H. Kim, A. Kobayashi, Y. Sasaki, T. Mori and H. Inokuchi, *Chem. Lett.*, 1988, 865.
21 G. Steinmecke, H. J. Sieler, R. Krimes and E. Hoyer, *Phosphorus, Sulfur Relat. Elem.*, 1979, **7**, 49.
22 teXsan for Windows: single crystal structure analysis software. Ver. 1.06, Molecular Structure Corporation, 1999. For ORTEP drawings, L. J. Farrugia, *J. Appl. Crystallogr.*, 1997, **32**, 565.
23 (*a*) A. J. Berlinsky, J. F. Carolan and L. Weiler, *Solid State Commun.*, 1974, **15**, 795; (*b*) R. H. Summerville and R. J. Hoffmann, *J. Am. Chem. Soc.*, 1976, **98**, 7240; (*c*) T. Mori, A. Kobayashi, Y. Sasaki, H. Kobayashi, G. Saito and H. Inokuchi, *Bull. Chem. Soc. Jpn.*, 1984, **57**, 627.